Pergamon

Journal of Structural Geology, Vol. 17, No. 12, pp. 1707 to 1724, 1995

0191-8141/95 $9.50+0.00

0191-8141(95)00059-3

Reverse modelling of detachment folds; application to the Pico del Aguila anticline in the South Central Pyrenees (Spain)

JOSEP POBLET and STUART HARDY

Fault Dynamics Project, Department of Geology, Royal Holloway, University of London, Egham Hill, Egham, Surrey TW20 0EX, U.K.

(*Received* 10 *June* 1994; *accepted in revised form* 8 *May* 1995)

Abstract—A simple method to estimate fold-amplification and thrust-movement rates for detachment folds is documented and illustrated by its application to a symmetrical detachment fold in the Southern Pyrenees, Spain. The technique provides a complete record of the kinematic evolution of detachment folds and is based on the application of equations for detachment folds involving limb rotation. The method uses the stratal pattern of the syntectonic sediments and assumes that these growth strata were deposited horizontally, that the folds involve a homogeneous competent unit detached over a ductile horizon, and that the folds can be represented by chevron-kink bands. The procedure is applicable to any detachment fold with associated growth strata that display wedge geometries ('progressive unconformities') indicating limb rotation through time. This method can be used for both detachment folds formed with constant limb length or variable limb length, and it can also accommodate undecompacted or decompacted growth strata.

INTRODUCTION

Syntectonic stratal patterns have been widely used to constrain the timing, deformation rates, kinematics and geometries of fault-related folds in many foreland fold-thrust belts (e.g. Medwedeff 1989, 1992, Mount *et al.* 1990, DeCelles *et al.* 1991, Bloch *et al.* 1993, Shaw & Suppe 1994). These tectono-sedimentary relationships have been well documented for fault-bend and fault-propagation folds (Suppe *et al.* 1992, Hardy & Poblet 1995). Much less is known of stratal patterns associated with detachment folds although they are a common feature of external parts of fold and thrust belts. Detachment folds form where there is a suitable detachment level, commonly evaporites or shales, and develop contemporaneously with a propagating blind thrust that follows the ductile horizon (Jamison 1987). When thrust-related folding takes place in submarine environments and sedimentation rates are high enough, structural and stratigraphic relationships of the resultant growth and pre-growth strata can provide crucial information about the timing and kinematics of fold-growth and thrust-slip rates (Medwedeff 1989). Until recently, the usual way to study the kinematics of fault-related folds using growth strata geometries has been by generating forward models (Mount *et al.* 1990). The main objective of this paper is to show that quantitative analysis of detachment folds is also possible by two dimensional reverse modelling using a simple geometric approach. The technique is based on the assumption that detachment fold limbs rotate through time according to the equations of Hardy & Poblet (1994). Combining the geometric configuration of growth strata with the equations for detachment folds derived by Hardy & Poblet (1994), fold-amplification and thrust-slip rates and the kinematic evolution of detachment folds can be determined. The proposed geometric model is tested by its application to the Pico del Aguila anticline, a superbly exposed detachment fold in the External Sierras, Pyrenees, Spain.

KINEMATIC MODELS FOR SYMMETRICAL DETACHMENT FOLDS DEVELOPED BY LIMB ROTATION

In contrast with self-similar models of fault-related folds, where the limb dips are attained instantaneously and do not change during fold amplification (e.g. Suppe 1983, Suppe & Medwedeff 1990), two models have been proposed to account for the geometry and kinematics of individual detachment folds formed by limb rotation. These two models assume that the folds involve a competent unit detached over a ductile horizon and that they develop above the tip line of a bed-parallel thrust. Both models have different implications in terms of structural evolution. In the first model (De Sitter 1956), folds grow by gradual increase in limb dip whereas the limb length remains constant (Fig. 1). Fold boundaries nucleate in their final positions relative to the competent unit, and shortening takes place by bedding rotation. The axial surfaces rotate to maintain constant stratigraphic thickness. In the second model (Dahlstrom 1990), fold limbs become longer as dip increases and folds grow (Fig. 1). This approach predicts that structures nucleate as small-wavelength folds, and shortening is accommodated by both outward migration of the axial surfaces and limb rotation. As in the first model, axial surfaces rotate to keep constant stratigraphic thickness. The equations for the kinematics of an homogeneous competent unit involved in a De Sitter (1956) type fold were derived by Hardy & Poblet (1994) (equations 1, 2 and 4). The

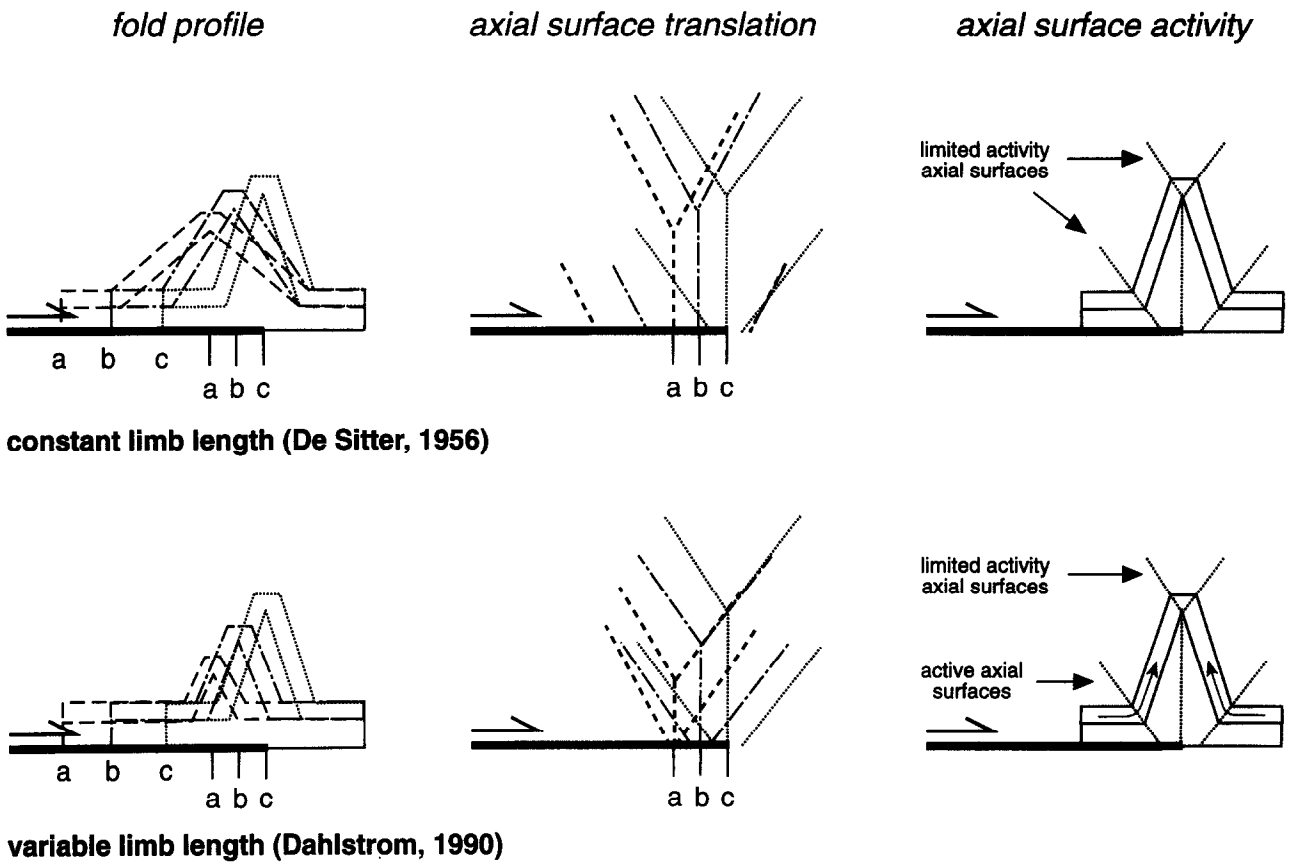

Fig. 1. Kinematic models for constant and variable limb length detachment folds formed by limb rotation.

assumptions of their model were that folds could be approximated by kink-like folds, that each bend had a constant interlimb angle throughout the whole competent unit, and that layer-parallel strain was negligible and all the contraction was accommodated by folding. The equations derived by Hardy & Poblet (1994) to describe the rotation of a single limb of a constant limb length detachment fold are also applicable to a variable limb length detachment fold. However, in this case another equation, based on Chamberlin (1910)'s law, has to be used to calculate the depth to detachment (see Dahlstrom 1990 for details and Appendix for development of the equation):

$$SZ = L^2 \cos \vartheta \sin \vartheta, \qquad (1)$$

where S is the slip along the detachment, Z is the depth to detachment, L is the limb length and ϑ is the rotation angle (Fig. 2). This equation implies that the area of the fold core (right hand side of the equation) equals the product of the slip (S) and the depth to detachment (Z). The application of this equation assumes several conditions which must be satisfied (Epard & Groshong 1993): (1) the décollement surface must be planar and parallel to the bedding of the non-deformed rocks in the hangingwall; (2) the depth to detachment must not change during fold evolution (the original regional elevation is not shifted vertically due to thinning by migration of the ductile unit towards the cores of the anticlines); and (3) no material must enter or leave the cross-section during folding (the area of the ductile unit is assumed to be constant).

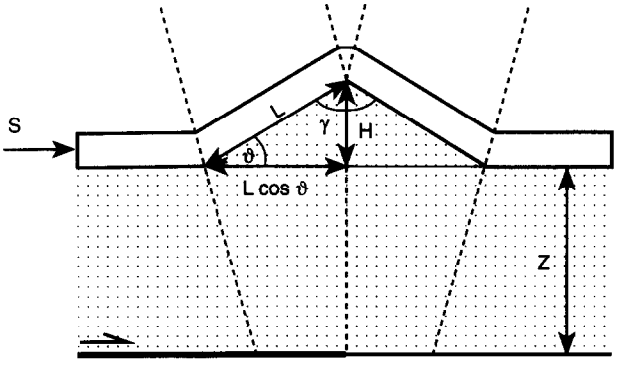

Fig. 2. Parameters involved in the calculation of limb rotation for a symmetrical chevron detachment fold; S = slip, H = uplift, γ = interlimb angle, L = limb length, ϑ = rotation angle, Z = depth to detachment.

The motion of the axial surfaces during fold evolution shows significant differences between the two detachment fold models. In De Sitter's approach, the axial surface that defines the lower end of the forelimb progressively rotates, but is pinned at the base of the competent unit. All other axial surfaces undergo rotation and translation over the blind thrust (Fig. 1). In the Dahlstrom approach, all the axial surfaces undergo rotation and forward translation (Fig. 1). On the basis of the activity of the axial surfaces, two types of axial

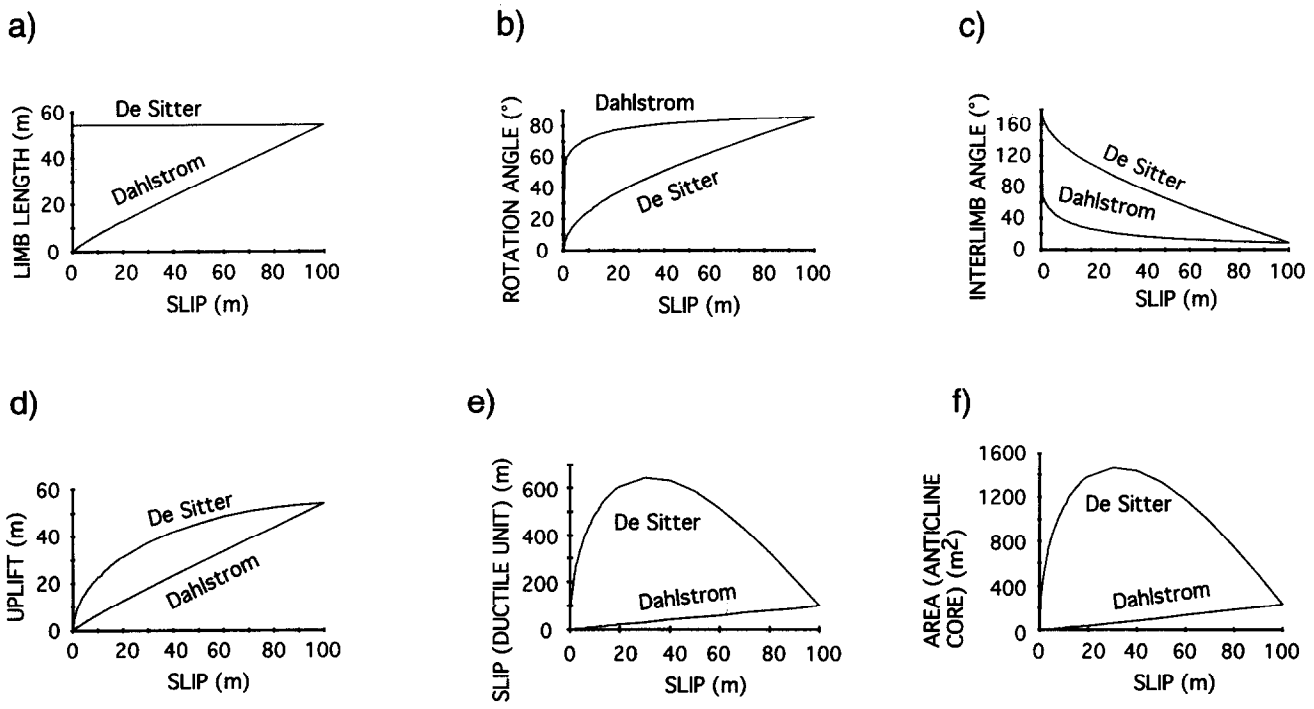

Fig. 3. Evolution of the different geometrical parameters for detachment folds.

surfaces can be distinguished in detachment folds: (a) limited activity axial surfaces which are pinned at the base of the competent unit, so that material motion through the axes is very limited and due only to the rotation of the axial surfaces; and (b) active axial surfaces through which material passes freely (Suppe *et al.* 1992). In De Sitter's approach, all the axial surfaces are limited activity axial surfaces (Fig. 1), whereas in the Dahlstrom approach the axial surfaces that define the anticlinal crest are limited activity axial surfaces and the other two axial surfaces are active axial surfaces (Fig. 1).

To better visualize the evolution of detachment folds, we have plotted the basic geometric parameters vs shortening for the two symmetrical chevron detachment folds shown in Fig. 1 (Fig. 3). Each fold is formed by equal incremental displacement units until a total shortening of 100 units is achieved along the basal detachment. Although constructed according to different models, both folds display identical final geometry. Using De Sitter's model, the limb length is always constant, whereas in the Dahlstrom approach the limb length increases almost linearly with increasing slip along the basal detachment (Fig. 3a). In the De Sitter model, both the rotation angle and the interlimb angle vary approximately in a linear fashion, with a slightly higher rate in the first stages (Figs. 3b & c). However, in the Dahlstrom approach, a huge variation is produced in the first stages, and afterwards the curves become almost asymptotic to the shortening axis (Figs. 3b & c). This indicates that, in the last fold amplification stages, large increases in the shortening induce small increases in the rotation and interlimb angles. In De Sitter's approach, uplift increases according to a function that decreases in gradient with increasing shortening (Fig. 3d). In the Dahlstrom model, increases in shortening are accompanied by almost linear increases in uplift. The Dahlstrom approach is based on the law of conservation of area for both the competent and the ductile units, i.e. the shortening is the same in both the competent and the ductile unit (Fig. 3e). Therefore, the anticline core area increases linearly with increasing shortening (Fig. 3f) and the slope of the function is the depth to detachment (see equation 1). Alternatively, in De Sitter's model, the area of the ductile unit is not conserved, thus shortening in the ductile unit and the anticline core area increase to a maximum and then decrease (Figs. 3e & f).

The manner in which a fold evolves, and in particular the activity of the axial surfaces, affects the development of microstructures and the distribution of fractures and breccia zones (Fischer *et al.* 1992). In folds formed with constant limb length (De Sitter 1956), all the axial surfaces are limited activity axial surfaces (Fig. 1). Therefore, only restricted areas around the present-day axial surfaces are expected to be fractured and deformed. This is because these areas are zones of maximum curvature, which are the loci of plastic yielding. If the De Sitter type model has been the dominant folding mechanism, we should not expect to find microstructural evidence for mobile axial surfaces in the fold limbs. In folds formed with variable limb length (Dahlstrom 1990), the axial surfaces that define the lower ends of the anticline limbs are active axial surfaces (Fig. 1). Therefore, as the limb length increases, the folded panels roll through these axial surfaces. During folding, each volume of rock added to the limbs undergoes the same strain as it passes through the axial surface and is rotated. Therefore, deformation should be distributed over the fold limbs and microstructures indicating the occurrence of mobile hinges may be present in both limbs.

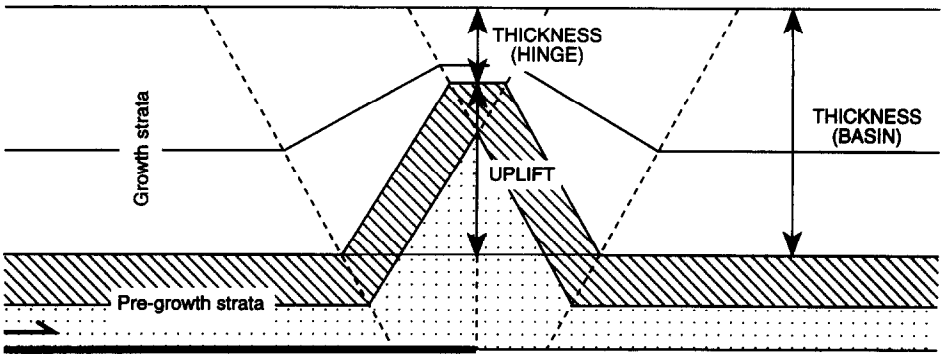

Fig. 4. Determination of the uplift of a symmetrical chevron fold during the deposition of a particular syntectonic unit using thicknesses of growth strata.

METHODOLOGY TO ESTIMATE FOLD-AMPLIFICATION AND THRUST-MOVEMENT RATES

The data needed to apply the method outlined below are: thicknesses of the syntectonic units in the basins and in the hinges of the folds, lithology of the units, ages of the boundaries that delimit the units and cross-sections of the folds which illustrate the original fold attitudes when they were formed.

If we assume that the growth strata were deposited horizontally, then by subtracting the cumulative thicknesses of growth strata in the hinge of the fold from the cumulative thicknesses of growth strata in the basin, we can calculate the uplift during the deposition of a particular bed according to the following equation (Fig. 4).

$$H = \sum_{i=1}^{n} \text{thickness basin} - \sum_{i=1}^{n} \text{thickness hinge}, \quad (2)$$

where H is the uplift of the fold. In order to apply equation (2), sedimentation must cover the fold at all times. When sedimentation rate is low (i.e. no sedimentation on the crest of the anticline), we assume that the uplift is at least the thickness of the syntectonic sediments in the basin. Therefore, in this case, the calculated uplift is a minimum value. Knowing the uplift during the deposition of a particular horizon, and assuming a kink-band like geometry for the fold, a constant limb length during fold growth (De Sitter 1956 model of detachment folding) and that internal deformation is negligible, equations (1), (2) and (4) of Hardy & Poblet (1994) can be applied to estimate the rotation angle, the slip along the detachment and the interlimb angle. By repeating this operation for different stratigraphic horizons of known age, plots of uplift, variation of the rotation angle, slip and interlimb angle through time can be constructed. The same procedure can be followed assuming that limb length has varied through time (Dahlstrom 1990 model of detachment folding). In this case, equation (1) has to be used to calculate the depth to detachment. Both geometrical models, constant or variable limb length through time, can be also used taking into account decompaction of growth strata.

APPLICATION TO A FIELD EXAMPLE

To test the method described above, it is now applied to a well-documented detachment fold in the Southern Central Pyrenees (Spain), the Pico del Aguila anticline (Fig. 5). Since ages, thicknesses, lithologies and geometries of the growth strata deposited during fold formation are known (Puigdefábregas 1975, Canudo *et al.* 1988, 1991, Hogan 1991, Barnolas *et al* 1992, Millán *et al.* 1994, Burbank *et al.* 1995), it is possible to date precisely the initiation and duration of deformation and to calculate rates of fold-amplification and thrust-slip. The estimation of thrust-displacement and fold-amplification rates allows us to propose a kinematic evolution for this detachment fold.

The Pico del Aguila anticline is located in the External Sierras, which are the emergent frontal part of the south Pyrenean thrust and fold belt. One of the most striking features of the External Sierras is the occurrence of N–S trending tight to isoclinal anticlines and broad box synclines (Fig. 5). In outline, the anticlines become smaller in amplitude westwards. Some of these regularly spaced structures can be described as lift-off folds, according to the definition of Mitra & Namson (1989), cored by Triassic rocks (Dobson 1990, Millán *et al.* 1994). The moderate northerly plunge of their axes has been interpreted to be the result of the folds' position over a N-dipping footwall ramp (Déramond *et al.* 1984, Cámara & Klimowitz 1985, McElroy 1990, Millán *et al.* 1994). Middle–Upper Eocene shallow marine and continental sediments show dramatic E–W changes in thickness over the anticlinal crests, showing that they are coeval to the uplift of the N–S folds (Soler & Puigdefábregas 1970, Puigdefábregas 1975, Anastasio 1987, Barnolas *et al.* 1992, Millán *et al.* 1994) (Fig. 5). Migration of the deformation towards the west is evident from the ages of the syntectonic sediments associated with the folds (Almela & Rios 1951, Soler & Puigdefábregas 1970, Puigdefábregas 1975, Anastasio 1987, Millán *et al.* 1994).

Two interpretations have been proposed to account for the formation of the N–S folds of the External Sierras: response to thrust movement (Séguret 1972, Millán *et al.* 1994, Martínez *et al.* 1995) and differential loading halotectonics (Anastasio 1987, 1992). Anastasio

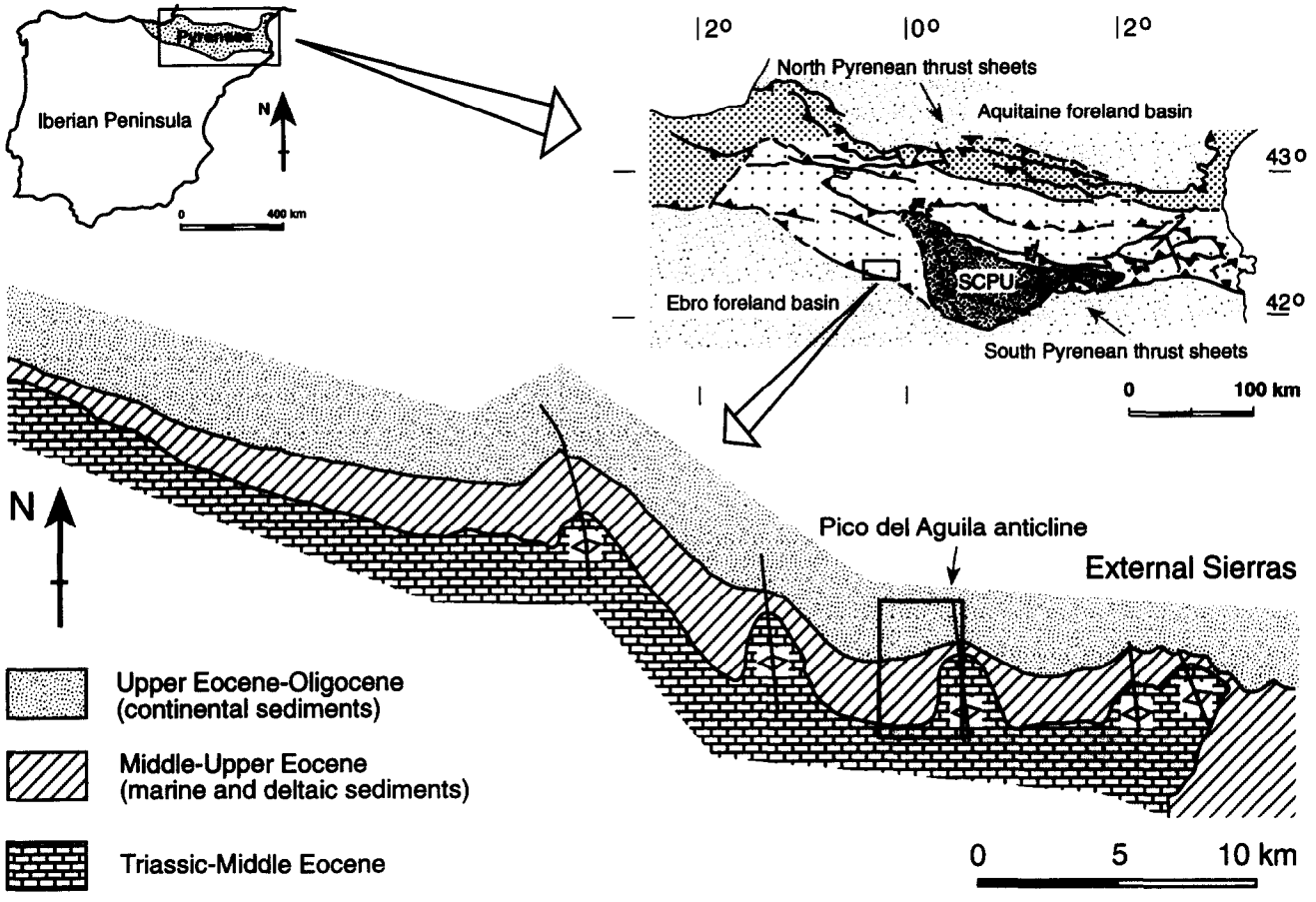

Fig. 5. Structural map of the Pyrenees (Muñoz 1992, modified) and simplified geological map of the External Sierras (Millán *et al.* 1994 modified) showing the location of the studied area (western limb of the Pico del Aguila anticline); SCPU = South Pyrenean Central Unit.

(1987, 1992) proposed that the N–S trending folds of the External Sierras developed in response to the differential load caused by the prograding Palaeogene clastic distributary systems. As a consequence, the mobile Triassic flowed from beneath the advancing sediment wedge towards the west, where thinner overburden and lower pressures occurred. Triassic evacuation in front of the wedge resulted in a trough that accommodated additional loading. Alternatively, Vendeville & Jackson (1992, p. 351) suggest that in the absence of regional extension (as in the case in the Pyrenees during the Eocene, Muñoz 1992), only very thin, brittle overburdens can be pierced if flanked by thicker sediments (sedimentary differential loading). However, in the External Sierras, the thickness of the overburden is 4.3–1.6 times the thickness of the ductile unit (760 m overburden, 175 m Triassic, Anastasio 1987; 960 m overburden, 600 m Triassic, Millán *et al.* 1994). Moreover, the ratio of overburden thickness to substrate thickness likely increases during fold growth because syntectonic sediments were continuously deposited on top of the pre-tectonic rocks (Puigdefábregas 1975, Barnolas *et al.* 1992, Millán *et al.* 1994). The ratio of brittle material thickness to mobile substrate thickness was possibly higher if we take into account that not all the Triassic consists of ductile rocks. Thus, according to the published stratigraphic sections, only between 44% (Anastasio 1987) and 78% (Millán *et al.* 1994) of the Triassic rocks are shales and gypsum, whereas the rest consist of limestones which deform in a more brittle fashion. We conclude that the above observations make Anastasio's hypothesis unlikely.

Séguret (1972), Millán *et al.* (1994) and Martínez *et al.* (1995) propose a different hypothesis to account for the N–S trending folds of the External Sierras. According to these authors, when the South Pyrenean Central Unit (Fig. 5) was displaced towards the south–southwest during Eocene and Oligocene time, it pushed and detached the footwall generating a set of frontal-oblique folds. As the South Pyrenean Central Unit advanced, the originally frontal-oblique structures located in the western margin of the thrust sheet rotated and new ones formed. This was due to a differential displacement of the South Pyrenean Central Unit, being maximum in the central part and decreasing towards the western margin (Dinarés 1992, Dinarés *et al.* 1992). East of the External Sierras, the N–S folds show arcuate geometries, from WNW–ESE trends in the north, to N–S trends to the south (see maps in Garrido 1973, Séguret 1972, Barnolas *et al.* 1991, Muñoz *et al.* 1994). The WNW–ESE orientations would correspond to the original orientation, whereas the north–south trends would be due to the progressive rotation of these originally frontal-oblique structures. Palaeographic reconstructions (Puigdefábregas 1975, p. 133), structural investigations (McElroy 1990, Millán *et al.* 1992) and palaeomagnetic data

(Hogan *et al.* 1988, Hogan 1991, Pueyo-Morer *et al.* 1994) document a clockwise rotation up to 50° for the External Sierras. Simply physical models (Millán *et al.* 1995) satisfactorily reproduce the clockwise rotation observed in the External Sierras. Therefore, we believe that the generation of the folds in the External Sierras can be better explained as induced mainly by shortening giving rise to thrusting and detachment folding. Shale and evaporite movement in the core of some N–S anticlines responsible for piercing the overlying strata (Anastasio 1987) would have been triggered by thrusting.

The Pico del Aguila anticline (Fig. 6) is a very well-exposed symmetrical isoclinal detachment fold (Millán *et al.* 1994), where both limbs show evidence of limb rotation. The pre-tectonic sequence consists of 600 m of Upper Cretaceous–Middle Eocene carbonates (Puigdefábregas 1975) that have detached on a Triassic succession of marls with intercalated evaporites, carnieules and dolomites (Almela & Rios 1951, Puigdefábregas 1975, Anastasio 1987, Dobson 1990, Millán *et al.* 1992, 1994). Overlying the pre-tectonic succession there is a syntectonic carbonate and clastic sedimentary package that has been divided into four lithostratigraphic units (Fig. 7) and several depositional sequences whose lithology and stratigraphy have been extensively described (Puigdefábregas 1975, Canudo *et al.* 1991, Barnolas *et al.* 1992, Millán *et al.* 1994). Biostratigraphic (Canudo *et al.* 1988) and magnetostratigraphic (Hogan 1991, Burbank *et al.* in press) data are also available. The four syntectonic units range in age from upper Lutetian to Priabonian. The oldest unit, which has been interpreted as a shallow open carbonate platform, consists of the upper part of the Guara limestones and is ascribed to the upper Lutetian (Canudo *et al.* 1988, Hogan 1991, Burbank *et al.* 1995). The Arguis marls range in age from Upper Lutetian to Bartonian (Hogan 1991, Burbank *et al.* 1995). They correspond to a distal platform whose depth decreased progressively, becoming a medium platform and a prodelta. The Belsue–Atares Unit is a clastic delta characterised by delta plain to delta front environments and ranges in age from Bartonian to Priabonian (Hogan 1991, Burbank *et al.* 1995). The uppermost unit, the Campodarbe Unit, is a fluviatile–lacustrine unit of Priabonian age (Canudo *et al.* 1988, Hogan 1991, Burbank *et al.* 1995).

Only the western limb of the Pico del Aguila anticline is analysed, as excellent exposures of this limb allow one to follow marker beds from the basin to the hinge of the fold (Fig. 6). In this limb, the growth strata sequence has been divided in several units bounded by marker beds (Fig. 7). Erosive truncations between the growth strata have not been recognized (Barnolas *et al.* 1992), but there is a progressive reduction in thickness of the growth strata towards the hinge of the anticline (Figs. 6 and 7). The syntectonic sediments exhibit a spectacular wedge geometry ('progressive unconformity' of Riba 1976) which opens away from the hinge of the anticline indicating that the folding took place by limb rotation (Figs. 6, 7 and 8). Internal deformation observed in the growth strata is limited to minor shearing on bedding planes, faulting on the pre-growth and growth strata contact, and some localized extensional faulting and cleavage in the hinge zone.

The pre-growth strata in the western limb of the Pico del Aguila anticline dip between 50 and 55° (Fig. 8). The fold axial surface is vertical and has a N–S strike, and the fold axis plunges about 30° to the north (Fig. 9). If it is assumed that the growth strata were deposited horizontally, it follows that the fold was formed with a flat-lying axis, because the growth strata in the core of the adjacent syncline presently dip about 30° to the north (Fig. 8) (similar to the fold axis plunge). In order to visualize the original attitude of the fold, a down-plunge cross-section perpendicular to the fold axis has been constructed following the method described by Wilson (1967) (Fig. 10). For ease of modelling the evolution of the fold geometry, the western limb is assumed to be a kink band (Fig. 11). The cross-section in Fig. 11 enables us to measure an average dip of the limb, the limb length of the fold, the uplift of the fold and the interlimb angle. Once the plunge of the fold is removed the western limb dips about 87°. Its present limb length is 1392 m and the uplift of the fold is 1391 m; the interlimb angle is about 6°.

The fact that in the Pico del Aguila detachment fold (a) fold growth took place by limb rotation; (b) the geometry of the pre-growth and growth strata display many of the characteristics seen in the theoretically modelled folds (Hardy & Poblet, 1994, Hardy *et al.* 1995); (c) the fold involves a competent unit (Upper Cretaceous–Middle Eocene) detached over a ductile unit (Triassic); and (d) internal deformation is negligible and therefore most of the contraction was accommodated by folding, allow us to apply the method outlined with some confidence to estimate thrust-slip and fold-amplification rates.

Before applying the method outlined, precise ages of the boundaries between the syntectonic units considered in this study (Figs. 7 and 10) need to be known. Magnetic analysis of samples collected in a stratigraphic section across the western limb and the hinge of the Pico del Aguila anticline allowed Hogan (1991) and Burbank *et al.* (1995) to locate magnetic polarity changes in the growth strata. The resulting magnetic polarity stratigraphy was correlated to the magnetic polarity time scale of Harland *et al.* (1990). The correlation was based upon biostratigraphic data supplied by Canudo *et al.* (1988) The magnetic polarity chron boundaries 13–19 were identified in the stratigraphic section. The ages of the boundaries of the syntectonic stratigraphic units were obtained by interpolation between polarity chron boundaries. Sources of errors in the time control offered by magnetostratigraphic dating include (Bentham 1992): measurement errors of stratigraphic thickness, non-unique correlation of the magnetic polarity stratigraphy with the magnetic polarity time scale of Harland *et al.* (1990), uncertainties associated with the exact placement of chron boundaries within the magnetic polarity stratigraphy and inherent errors in the absolute

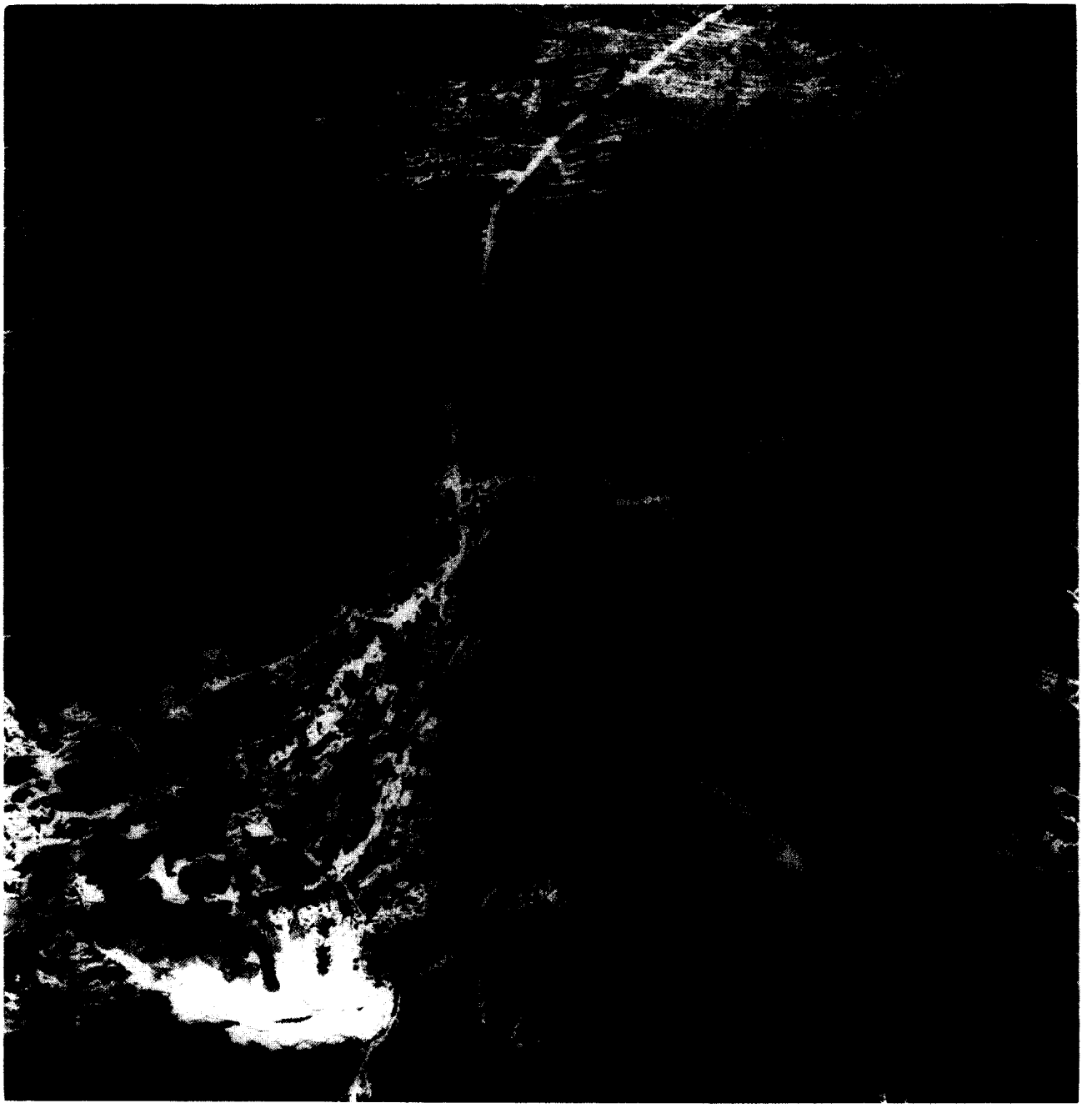

Fig. 6. Aerial photograph of the Pico del Aguila anticline, showing the dramatic thickness change of the growth strata over the crest of the anticline. The pre-growth strata correspond to the dark coloured area in the lower centre-right part of the photograph. The approximate size of the photograph is 4.9 × 4.9 km.

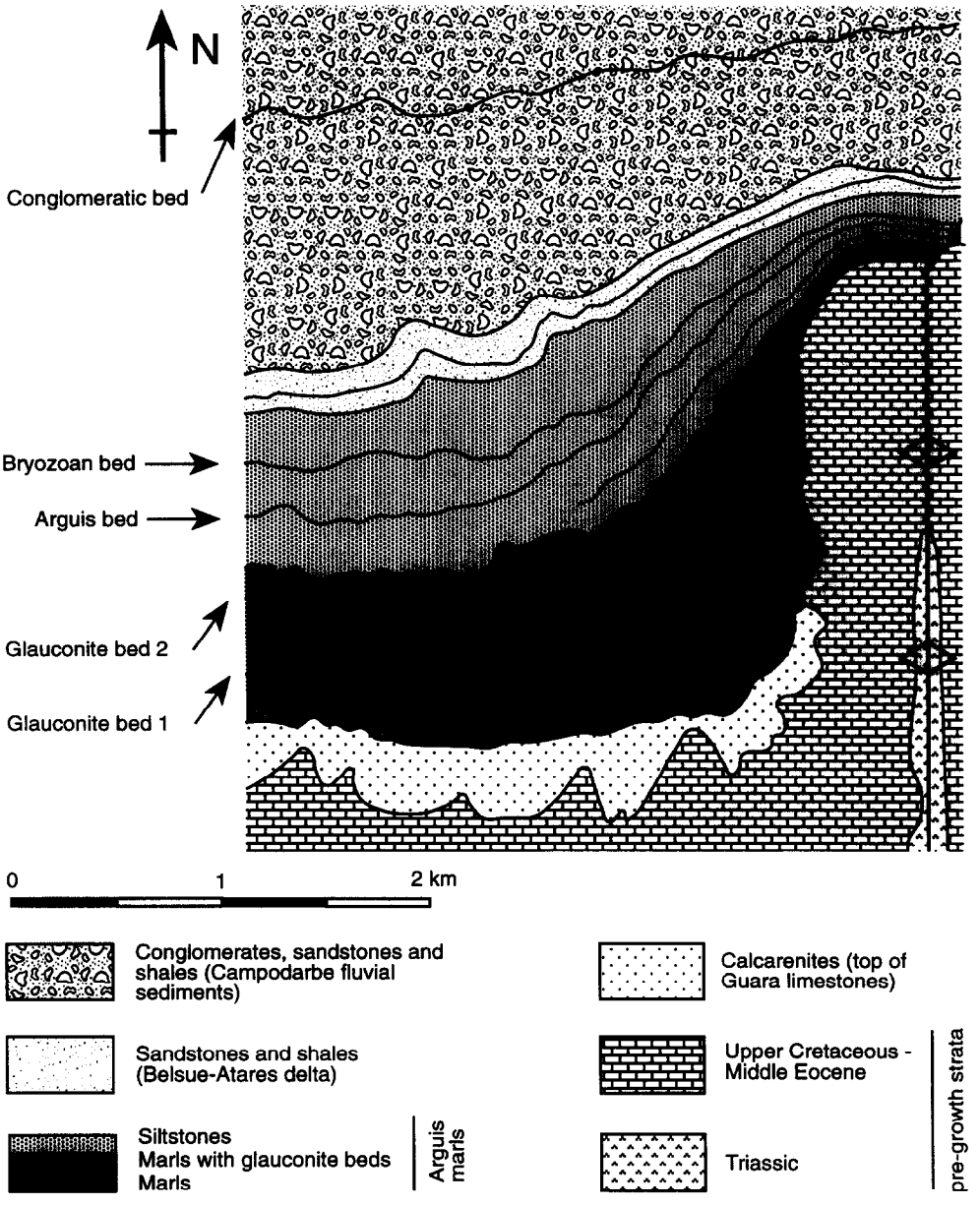

Fig. 7. Geological map of the western limb of the Pico del Aguila anticline showing the main marker beds and the stratigraphic units in which the growth strata have been divided.

ages of those boundaries as defined by Harland *et al.* (1990). Most of these errors are hardly quantifiable. To simplify, we will assume that no errors have been made in the measurement of the stratigraphic sections and that our correlation of the magnetic polarity stratigraphy with the magnetic polarity time scale is correct. Only uncertainties associated with the exact placement of chron boundaries within the magnetic polarity stratigraphy, due to the spacing of the sampling, are addressed. The maximum error estimated is in the location of the boundaries of chrons 17 and 18 at ±0.02 Ma.

Tables 1 and 2 display the results obtained using the thicknesses and the estimated ages of the growth units, and applying equations (1), (2) and (4) of Hardy & Poblet (1994) and (1) and (2) in this paper to the Pico del Aguila anticline. The uplift and variation of the limb length, rotation angle, interlimb angle and slip through time can be plotted (Fig. 12). Results can be calculated for both models: constant limb length and variable limb length, and also for undecompacted and decompacted growth strata. In order to decompact the growth strata, we used the decompaction algorithm proposed by Angevine *et al.* (1990) and the porosity constants given by Sclater & Christie (1980). This method of decompaction assumes that the porosity decreases with depth and that the volume of rock grains within the unit never changes. The original thickness of one rock unit is related to the present-day thickness as follows (Angevine *et al.* 1990):

$$T_o + \left[\left(\frac{\phi_o}{c}\right)(e^{(-cd_o)})(e^{(-cT_o)} - 1)\right] = T_N + \left[\left(\frac{\phi_o}{c}\right)(e^{(-cd_N)})(e^{(-cT_N)} - 1)\right], \quad (3)$$

where T_o is the thickness of the unit at some earlier time, ϕ_o is the porosity of the unit at some earlier time, c is the constant of each lithology, d_o is the depth to which the unit was buried at some earlier time, T_N is the present

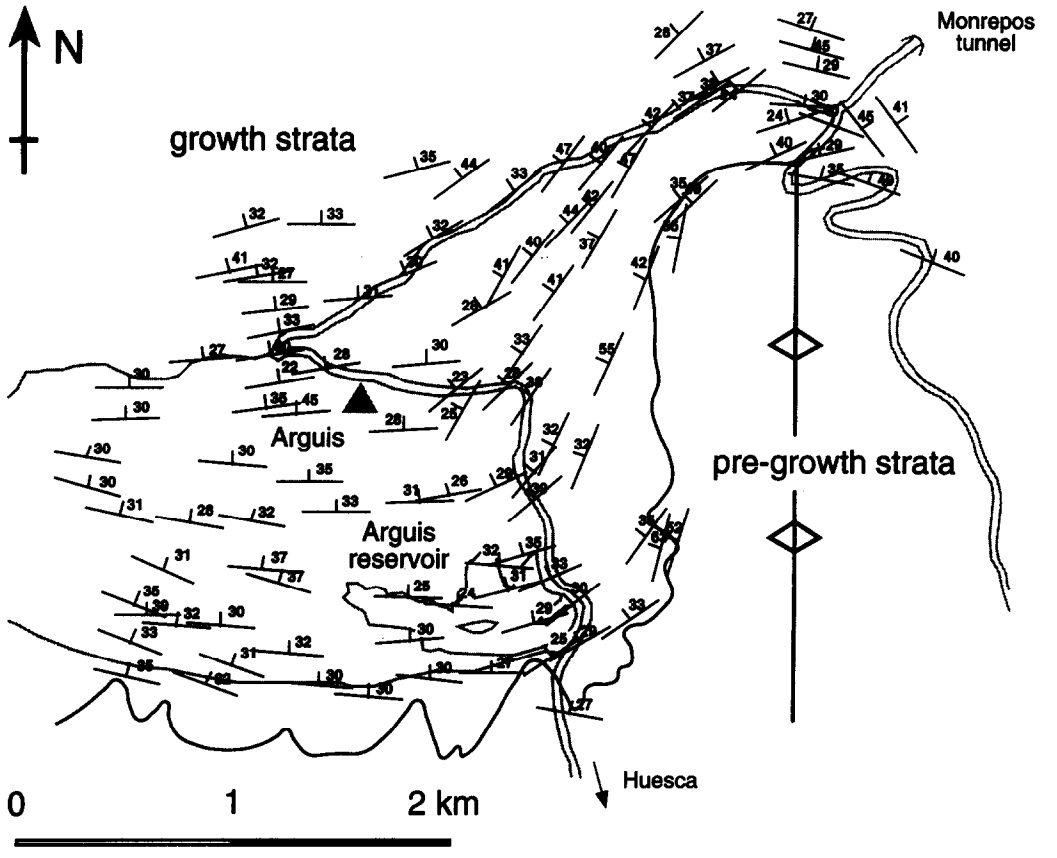

Fig. 8. Bedding dip map of the western limb of the Pico del Aguila anticline. Single thin lines = railroads, double thin lines = roads.

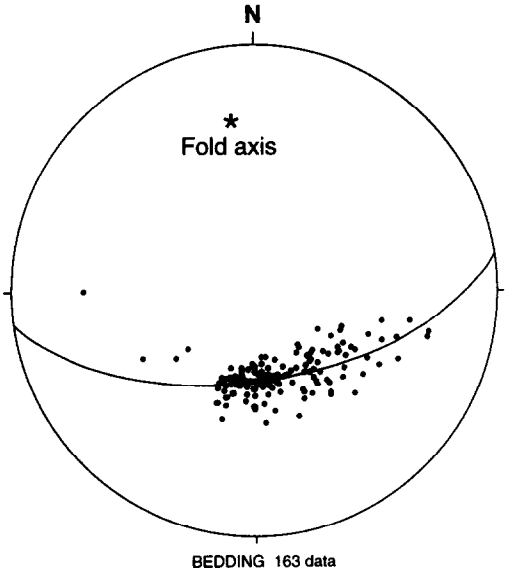

Fig. 9. Equal area plot of the poles to bedding measured in the western limb of the Pico del Aguila anticline. The fold axis is also shown. The computer program used to plot the data and to find the best-fit great circle is StereoPlot II written by R.A. Allmendinger.

thickness of the unit and d_N is the present depth to which the unit is buried. The change in unit porosity is assumed to be a simple exponential relationship (Sclater & Christie 1980):

$$\phi_N = \phi_o e^{(-cz)}, \quad (4)$$

where ϕ_N is the present-day porosity of the unit and z is the present depth of burial.

The main uncertainties in the determination of the geometric parameters required to model the kinematic evolution of the Pico del Aguila anticline (Tables 1 and 2) include: measurement errors of stratigraphic thickness giving rise to errors in the uplift, errors related to the decompaction procedure also influencing the uplift, cartographic errors and errors in the cross-section construction giving rise to uncertainties in the measurement of the limb length, and errors in the measurement of the limb length due to the approximation of the real fold to a kink-like fold using Wilson's method. Most of these errors are difficult to quantify. We will assume no errors in the measurement of the limb length. Only errors related to the uplift are addressed. Error bars associated with uplift are considered to be 10% of each value quoted.

Some considerations have to be made on the uplift and slip obtained in the graphs for the Pico del Aguila anticline. Sine the three lower syntectonic units onlap the fold limb (Figs. 7 and 10), it has been assumed that the uplift of the fold during the initial stages corresponds to the thickness of the growth strata in the basin. Therefore, the estimated uplift of the fold in these initial stages is a minimum value (Fig. 12). The first continuous marker bed that overlaps the Pico del Aguila anticline is the second glauconite bed (Figs. 7 and 10).

In some anticlines of the External Sierras piercement of the Upper Cretaceous–Eocene rocks by the underlying Triassic ductile rocks has been described (Anastasio 1987). In our calculations, all the uplift has been assumed

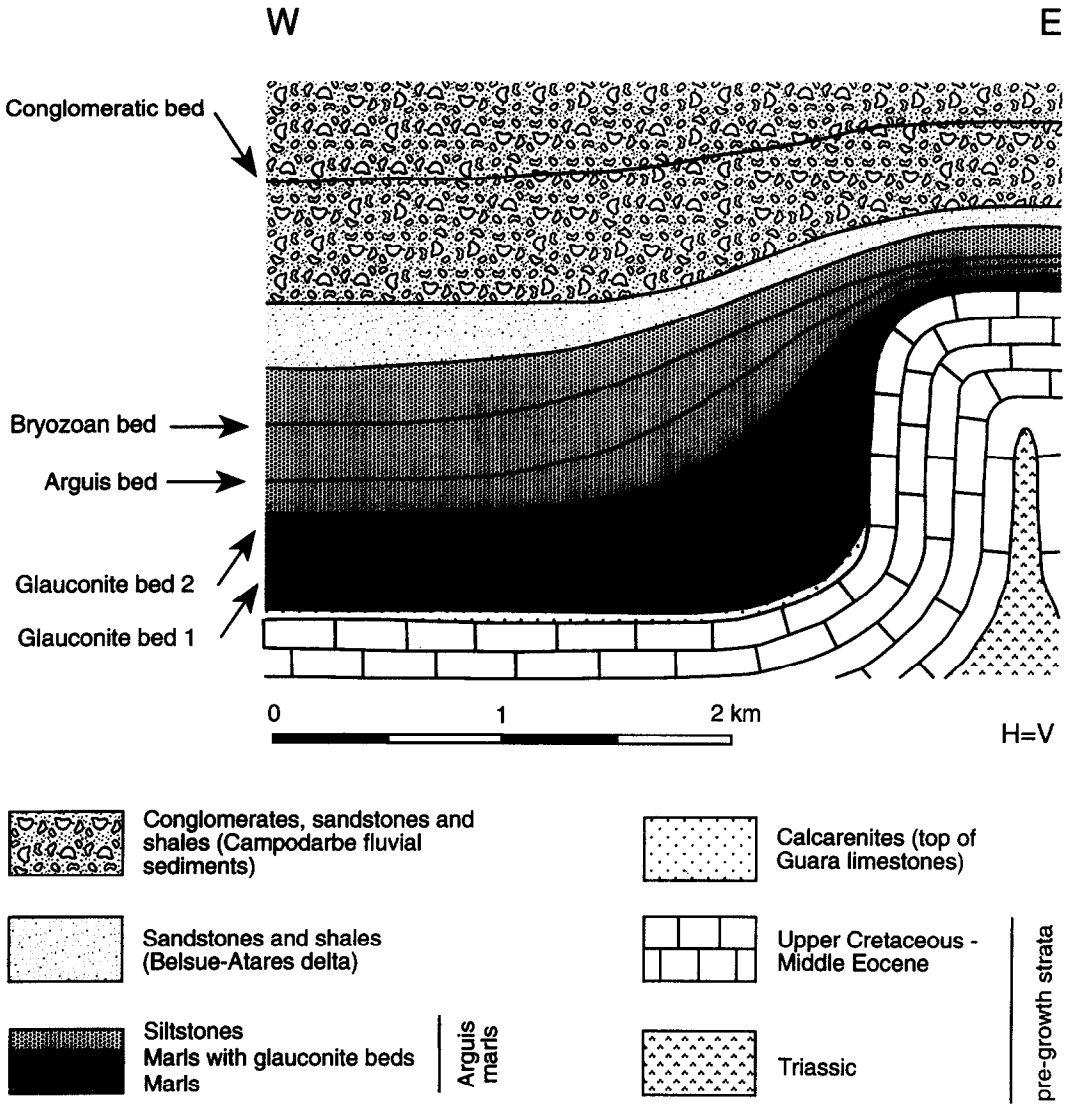

Fig. 10. Down-plunge projection of the western limb of the Pico del Aguila anticline.

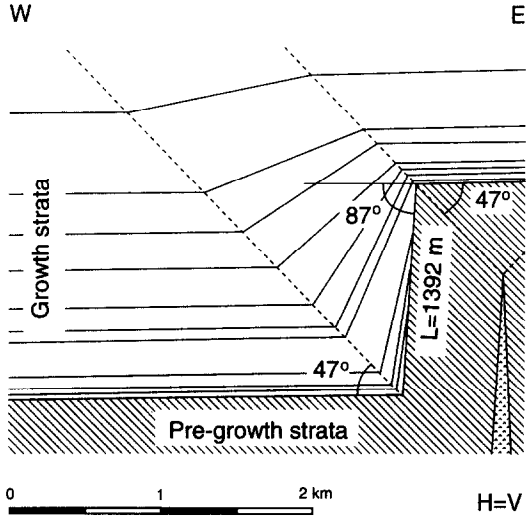

Fig. 11. Schematic section of the western limb of the Pico del Aguila anticline based on the cross-section on Fig. 10 but constructed using the kink-band method.

to be caused by tectonic shortening, giving rise to slip along the basal detachment transferred into detachment folding above the thrust tip. Evaporite piercement would cause fold uplift. Therefore, assuming evaporite piercement to occur in the formation of the Pico del Aguila anticline, our shortening values (derived from the uplift values) would be overestimations of the real tectonic shortening, as part of the uplift would have been due to evaporite piercement. Diapir growth can occur by upbuilding (active piercement) or downbuilding (passive piercement). In areas where the overburden is thick and strong, such as the Pico del Aguila anticline, diapir growth can only be achieved by regional extension or downbuilding (Jackson & Talbot 1994). During the Eocene, the Pyrenees experienced contractional deformation (Muñoz 1992). Jackson & Talbot (1994) proposed that downbuilding implies that the diapir increases by growing downward relative to the sedimentary surface. The base of the diapir subsides, together with surrounding strata, as the basin fills with sediment. In order for this mechanism to occur, the diapir crest should remain at or just below a thin roof, which is continually thickened by

Table 1. Values used in order to unravel the kinematic evolution of the Pico del Aguila anticline assuming a constant limb length detachment fold model; t = thickness, T = cumulative thickness, length = limb length, rotat = rotation angle, inter = interlimb angle.

	Constant limb length: Undecompacted beds									
Units	t Basin	T Basin	t Hinge	T Hinge	Age	Uplift	Length	Rotat	Slip	Inter
Conglomerate	535	1880	422	731	36.68±0.02	1149±114.9	1392	56±9	1212±405	69±19
Fluvials base	265	1345	46	309	38.28±0.02	1036±103.6	1392	48±7	925±260	84±14
Deltaics base	228	1080	125	263	39.14±0.02	817±81.7	1392	36±4	530±155	108±8
Bryozoan bed	253	852	24	138	39.89±0.02	714±71.4	1392	31±4	394±91	118±7
Arguis bed	126	599	82	114	40.71±0.02	485±48.5	1392	20±3	174±39	139±4
Marls-silts	89	473	32	32	41.12±0.02	441±44.1	1392	18±2	143±32	143±4
Glauconite 2	234	384	0	0	41.41±0.02	384±38.4	1392	16±2	108±23	148±3
Glauconite 1	82	150	0	0	42.17±0.02	150±15	1392	6±1	16±4	168±2
Marls	38	68	0	0	42.45±0.02	68±6.8	1392	3	3±1	174±1
Calcarenites	30	30	0	0	42.57±0.02	30±3	1392	1	1	178±1
Pre-growth	0	0	0	0	42.67±0.02	0	0	0	0	180

	Constant limb length: Decompacted beds							
Units	T Basin	T Hinge	Age	Uplift	Length	Rotat	Slip	Inter
Conglomerate	2270	950	36.68±0.02	1320±132.0	1392	71±12	1900±567	37±26
Fluvials base	1769	474	38.28±0.02	1295±129.5	1392	68±9	1763±501	43±23
Deltaics base	1527	420	39.14±0.02	1107±110.7	1392	53±7	1096±339	75±17
Bryozoan bed	1259	230	39.89±0.02	1029±102.9	1392	48±6	909±255	85±14
Arguis bed	926	192	40.71±0.02	734±73.4	1392	32±4	418±98	116±7
Marls-silts	761	56	41.12±0.02	705±70.5	1392	30±4	383±89	119±7
Glauconite 2	634	0	41.41±0.02	634±63.4	1392	27±3	306±69	126±6
Glauconite 1	277	0	42.17±0.02	277±27.7	1392	11±5	56±12	157±2
Marls	125	0	42.45±0.02	125±12.5	1392	5±1	11±3	170±1
Calcarenites	57	0	42.57±0.02	57±5.7	1392	2±1	2±1	175±1
Pre-growth	0	0	42.67±0.02	0	0	0	0	180

Table 2. Values used in order to unravel the kinematic evolution of the Pico del Aguila anticline assuming a variable limb length detachment fold model; t = thickness, T = cumulative thickness, length = limb length, rotat = rotation angle, inter = interlimb angle.

	Variable limb length: Undecompacted beds									
Units	t Basin	T Basin	t Hinge	T Hinge	Age	Uplift	Rotat	Length	Slip	Inter
Conglomerate	535	1880	422	731	36.68±0.02	1149±114.9	87±1	1150±115	2184±243	6±1
Fluvials base	265	1345	46	309	38.28±0.02	1036±103.6	87±1	1037±104	1969±209	6±1
Deltaics base	228	1080	125	263	39.14±0.02	817±81.7	86±1	819±81	1533±166	7±1
Bryozoan bed	253	852	24	138	39.89±0.02	714±71.4	86±1	716±71	1328±145	8±1
Arguis bed	126	599	82	114	40.71±0.02	485±48.5	84±1	488±48	875±98	12±1
Marls-silts	89	473	32	32	41.12±0.02	441±44.1	84±1	444±44	788±90	13±2
Glauconite 2	234	384	0	0	41.41±0.02	384±38.4	83±1	387±38	676±78	15±2
Glauconite 1	82	150	0	0	42.17±0.02	150±15	74±2	156±14	227±30	31±2
Marls	38	68	0	0	42.45±0.02	68±6.8	63±2	76±6	84±12	53±3
Calcarenites	30	30	0	0	42.57±0.02	30±3	50±2	39±3	28±4	81±4
Pre-growth	0	0	0	0	42.67±0.02	0	0	0	0	180

	Variable limb length: Decompacted beds							
Units	T Basin	T Hinge	Age	Uplift	Rotat	Length	Slip	Inter
Conglomerate	2270	950	36.68±0.02	1320±132.0	88±1	1321±132	2536±266	5±1
Fluvials base	1769	474	38.28±0.02	1295±129.5	88±1	1296±128	2486±260	5±1
Deltaics base	1527	420	39.14±0.02	1107±110.7	87±1	1108±111	2111±223	5±1
Bryozoan bed	1259	230	39.89±0.02	1029±102.9	87±1	1030±103	1955±208	6±1
Arguis bed	926	192	40.71±0.02	734±73.4	86±1	736±73	1368±148	8±1
Marls-silts	761	56	41.12±0.02	705±70.5	86±1	707±70	1311±142	8±1
Glauconite 2	634	0	41.41±0.02	634±63.4	85±1	636±63	1170±128	9±1
Glauconite 1	277	0	42.17±0.02	277±27.7	80±1	281±27	468±56	19±2
Marls	125	0	42.45±0.02	125±12.5	72±1	131±12	182±24	36±3
Calcarenites	57	0	42.57±0.02	57±5.7	60±2	66±5	66±10	59±4
Pre-growth	0	0	42.67±0.02	0	0	0	0	180

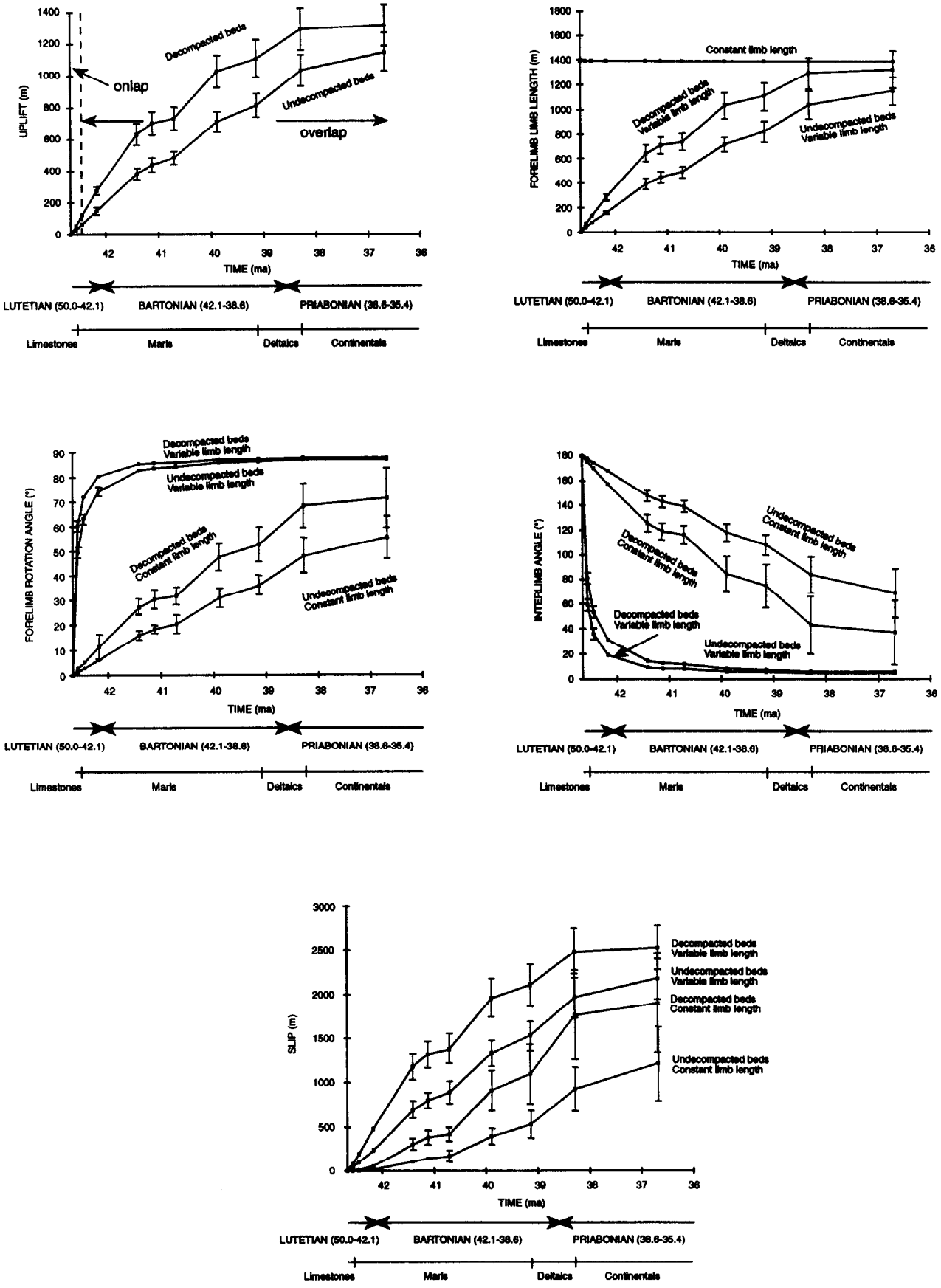

Fig. 12. Graphs of uplift, variation of the limb length, rotation angle, interlimb angle and slip vs time for the Pico del Aguila anticline. Small error bars have not been drawn.

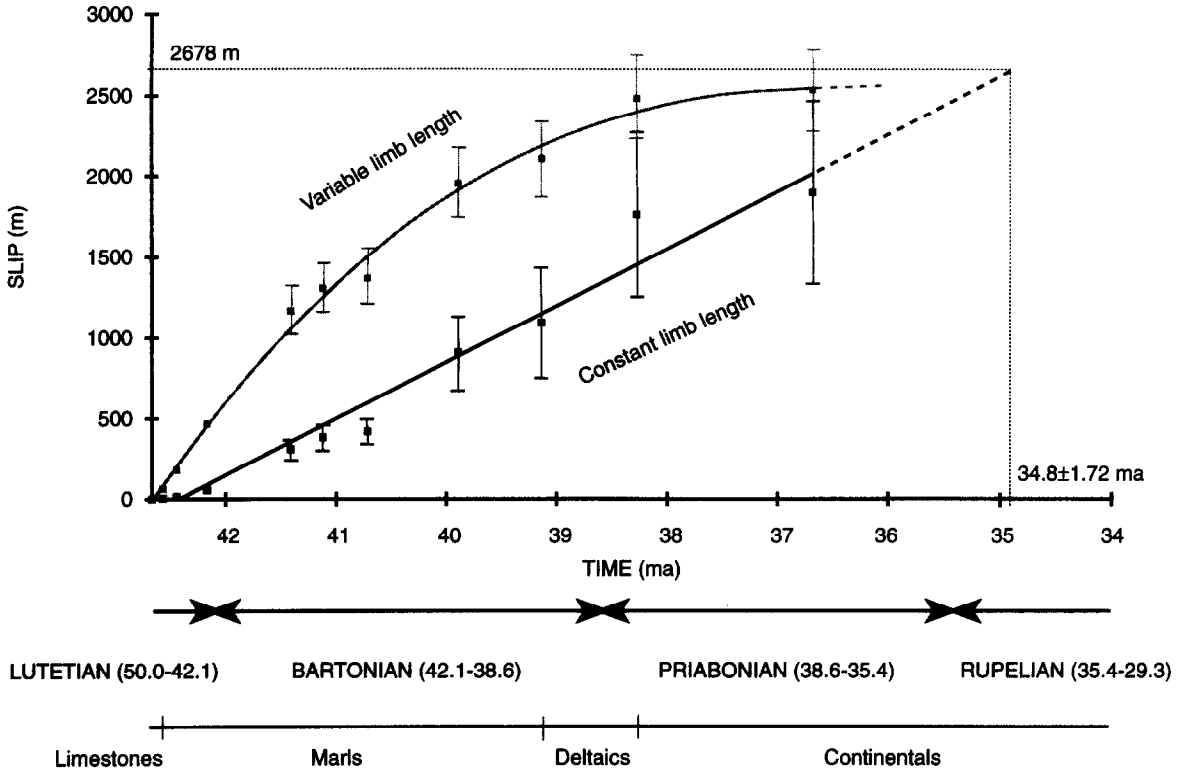

Fig. 13. Best-fit curves for variation of the slip vs time for decompacted beds in the Pico del Aguila anticline (constant and variable limb length detachment fold models). Small error bars have not been drawn.

sedimentation and thinned by erosion or extensional thinning. As there was little erosion of the anticline crest of the Pico del Aguila fold (Barnolas *et al.* 1992) the Triassic rocks do not remain at or just below a thin roof, but below a 600 m thick series of limestones and sandstones (Puigdefábregas 1975). The thickness of the sediments at the anticline crest increases as syntectonic sediments are deposited and not removed by erosion. Therefore, we conclude that growth of the Pico del Aguila anticline by downbuilding could have occurred, but was of minor importance.

In the Pico del Aguila anticline, it is difficult to precisely identify the boundary between growth and post-growth strata. In the last stages (i.e. during the deposition of the Campodarbe fluvial sediments), thickness variations between growth strata deposited in the basin and on the hinge are very small and therefore difficult to determine. However, the timing of cessation of tectonic activity can be inferred. The present uplift of the fold is 1391 m, and the rotation and the interlimb angles are 87° and 6° respectively. Assuming that all the shortening was taken up by limb rotation, in order to achieve these values (uplift, rotation and interlimb angles) the E–W slip needed using the equations presented in this paper is approximately 2678 m. From the slip vs time plots for decompacted beds we can determine the best-fit curves, which are a linear function in the case of a detachment fold formed with constant limb length (Fig. 13):

$$S = (-351.55 \pm 104.38t) + (14911 \pm 4419), \quad (5)$$

and a third order polynomial function in the case of a detachment fold formed with variable limb length (Fig. 13):

$$S = (-4.1744 \pm 0.7227t^3) + (414.83 \pm 77.3t^2) - (13594 \pm 2759t) + (149062 \pm 33128), \quad (6)$$

where S is the slip in m and t is the time in Ma. According to the best-fit function, in the case of a constant limb length detachment fold, a value of slip of 2678 m (end of deformation in the Pico del Aguila anticline) would have been achieved at approximately 34.8 ± 1.72 Ma (lower part of the Rupelian, Oligocene, or upper part of the Priabonian, Eocene) during the deposition of the Campodarbe Unit. Therefore, the total shortening responsible for the formation of the Pico del Aguila anticline would have lasted approximately 7.87 ± 1.74 Ma, from 42.67 ± 0.02 to 34.8 ± 1.72 Ma. Unfortunately, in the case of a variable limb length detachment fold, the best-fit function obtained does not correctly predict the slip before 36.68 ± 0.02 Ma. According to this curve, the slip decreases from 36.68 ± 0.02 Ma to the present day. However, taking into account the error bars for the slip vs time data (Fig. 13), the end of deformation of the Pico del Aguila anticline could have been achieved during the deposition of the conglomeratic bed of the Campodarbe Unit (36.68 ± 0.02 Ma).

In the case of detachment folds formed with constant limb length, the slip vs time best-fit function obtained for the Pico del Aguila anticline is linear (equation 5). The slope of the function corresponds to a constant rate of 0.35 ± 0.1 mm a^{-1}. In the case of detachment folds formed with variable limb length the gradient of the slip vs time best-fit function is the derivative of equation (6):

$$\frac{d(-4.1744 \pm 0.7227t^3 + 414.83 \pm 77.3t^2 - 13594 \pm 2759t + 149062 \pm 33128)}{dt}$$

$$= (-12.5232 \pm 2.1681t^2) + (829.66 \pm 154.6t) - (13594 \pm 2759). \quad (7)$$

According to this function, the maximum slip rate took place during the first stages of growth (0.99 ± 0.01 mm a^{-1}) but it decreased progressively to very low values during the last stages (Fig. 13).

Our analysis has produced quantitative data on fault-slip and fold-amplification rates, and can also predict long term rates of fault-slip using empirical relationships. Therefore, in areas where seismicity related to growth fault-related folding takes place (e.g. structures related to the movement of the San Andreas fault in California described by Medwedeff 1989, 1992, Bloch *et al.* 1993) the method outlined can help in the assessment of hazards posed by active, seismogenic faults (Shaw & Suppe 1994).

The uplift per unit time of the Pico del Aguila anticline decreases with time. The maximum uplift rate (0.31 ± 0.08 mm a^{-1}) took place during the first growth stages. In the last stages, the slope of the uplift vs time curve is very gentle, indicating that the uplift increment is small (Fig. 12). This implies that for a model of constant limb length detachment fold, although the slip is constant (Fig. 13), the uplift rate decreases with time. In the case of constant limb length detachment folds formed with constant slip rate, the beds deposited during the last stages of growth, when the uplift rate is small, are usually sub-horizontal and hardly show thickness variations across the fold. They are, however, still growth strata deposited during further growth fold deformation. Therefore, it must be noted that, although the younger growth strata are almost flat-lying and exhibit approximately constant thickness, this does not necessarily imply that the tectonic activity is decreasing. It may simply be the result of the nonlinearity in the system, i.e. constant slip rate causes a decreasing uplift rate. Alternately, the fact that these uppermost growth strata units display gentle dips and almost no thickness changes makes it difficult to precisely locate the boundary between syn- and post-tectonic sediments. For a model of variable limb length detachment fold, since the slip rate decreases through time (Figs. 12 and 13), the uplift rate also decreases. Situations similar to those described for constant limb length detachment folds developed with constant slip rate occur in the case of variable limb length detachment folds when the slip rate decreases with time and therefore the uplift rate also decreases with time. In these cases, the uppermost growth strata also exhibit gentle dips and almost no thickness variations, making it difficult to identify the boundary between growth and post-growth strata.

Using the data obtained, the sequential development of the Pico del Aguila anticline as a detachment fold with constant (Fig. 14) and variable (Fig. 15) limb length has been modelled. The present-day geometry is shown in Fig. 11. In the theoretical model of Fig. 14 all the shortening is taken up by limb rotation, whereas in the theoretical model of Fig. 15 the shortening is taken up by limb rotation and limb lengthening. The growth sediments initially deposited in the basin west of the fold rotate, increasing their dip, by rolling through the limited activity axial surfaces in the case of constant limb length detachment folds, and through the active axial surfaces in the case of variable limb length detachment folds. The axial surfaces decrease their dip in order to keep constant stratigraphic thickness for the pre-growth strata. In this way, the sediments initially deposited in the basin are progressively incorporated into the fold limb. The structure locks up when the limbs become vertical. Since the sedimentation rate is approximately constant (Fig. 16) but the uplift per unit time decreases with time (Fig. 12), the kinematic evolution of the Pico del Aguila anticline consists of a quick overlap after the initial stages of onlap (Figs. 14 and 15). On the basis of the available field data, it is not possible for us to decide which of the two models presented operated in the case of the Pico del Aguila anticline. This issue is the subject of ongoing research.

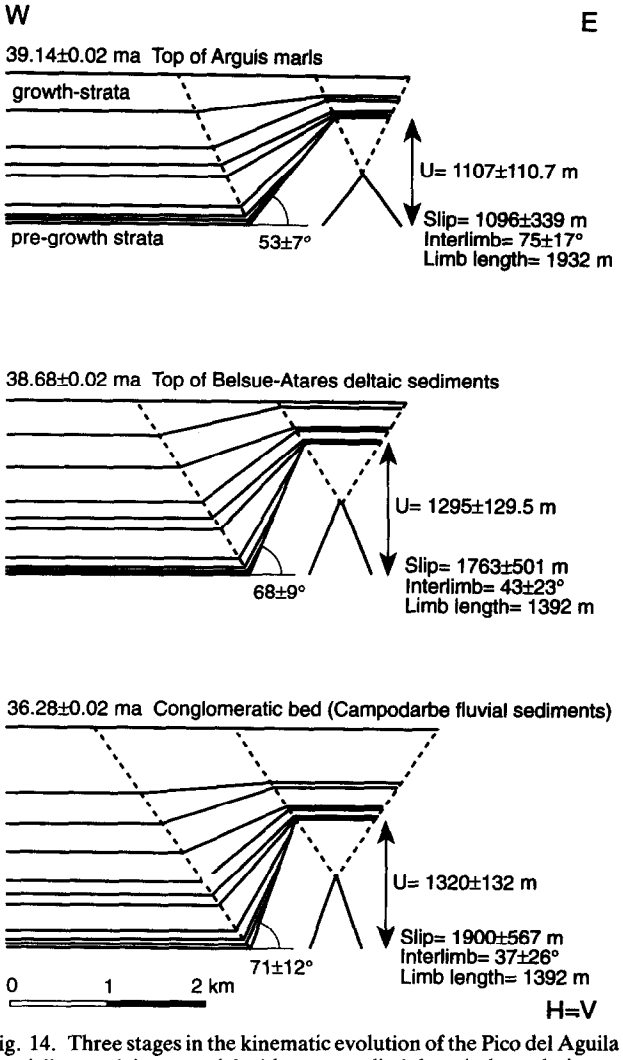

Fig. 14. Three stages in the kinematic evolution of the Pico del Aguila anticline applying a model with constant limb length through time.

According to Séguret (1972), Millán *et al.* (1994) and

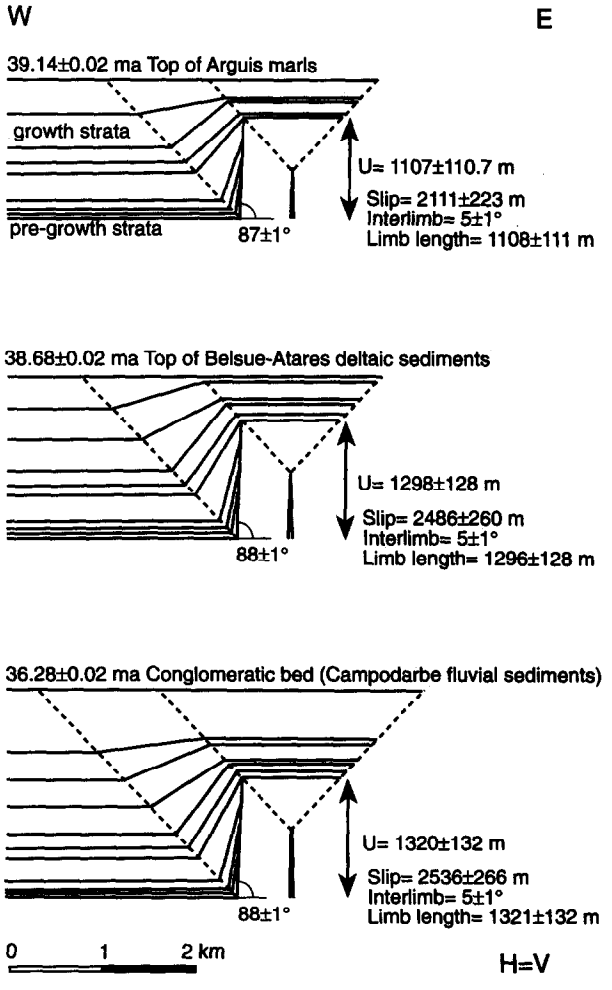

Fig. 15. Three stages in the kinematic evolution of the Pico del Aguila anticline applying a model with variable limb length through time.

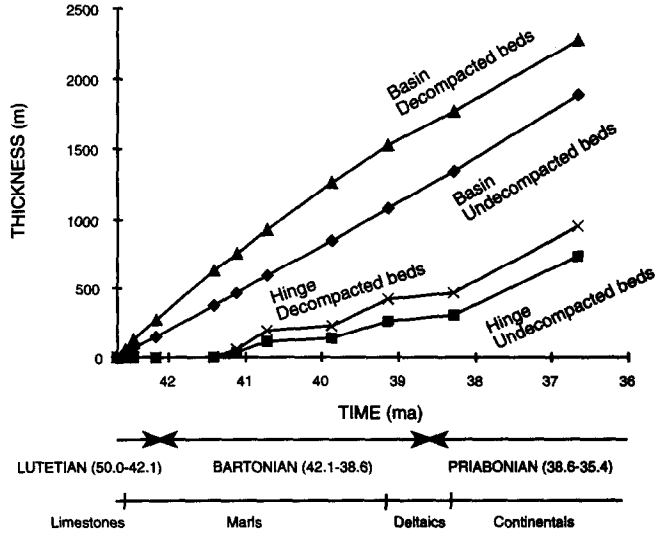

Fig. 16. Graph of thickness of growth strata vs time for the Pico del Aguila anticline.

Martínez *et al.* (1995) the present N–S trending folds of the External Sierras are footwall, frontal-oblique structures related to the South Pyrenean Central Unit. As this thrust sheet advanced towards the south–southwest during the Eocene–Oligocene, the folds developed in the western margin of the South Central Pyrenean Unit rotated to a N–S trending attitude. The average thrust movement rate estimated for the Pico del Aguila anticline (≤ 1 mm a^{-1}) is much lower than the slip rates of 2.1–4.0 mm a^{-1} estimated using balanced sections in similar structural positions along the eastern oblique ramp of the South Central Pyrenean Unit (Fig. 5), during similar time intervals (Burbank *et al.* 1992). This remarkable difference in the shortening rate may be due to the fact that we are only considering one particular structure, whereas Burbank *et al.* (1992) calculated the total shortening along the eastern oblique ramp of the South Central Pyrenean Unit involving an imbricate stack of thrust sheets. At present, the Pico del Aguila anticline is located about 60 km west from the western margin of the South Central Pyrenean Unit itself (see maps in Anastasio, 1987, 1992, Martínez *et al.* 1995, Millán *et al.* 1995) and therefore the slow rates obtained might indicate a decrease in the strain rate as deformation propagated towards the foreland.

CONCLUSIONS

(1) The application of the equations proposed for detachment folding to well-constrained field examples provides new insights into the kinematics of deformation (relationships between amount of slip, uplift and limb rotation for constant and variable limb length detachment folds), as well as the rates of fold growth and thrust-slip in detachment folds. A similar approach to the one proposed in this paper can be applied to other types of fault-related folds with growth strata using the appropriate algorithms (i.e. fault-bend and fault-propagation folds) in order to derive fold-amplification and thrust-movement rates.

(2) The method described can be applied to the assessment of seismic risks in areas where active fault-related folding and synchronous sedimentation is occurring, because it offers the potential of establishing long term rates of fault-slip.

(3) In growth detachment folds formed with constant limb length and approximately constant slip and sedimentation rates, the boundary between syn- and post-tectonic sediments can be difficult to ascertain precisely. This is due to the fact that, although the slip is constant through time, the uplift decreases dramatically in the last stages of growth. Therefore, the sediments deposited in the last stages of fold amplification are approximately flat-lying and do not exhibit significant thickness variations across the fold. However, these sediments were still deposited during tectonic activity and do not imply a decrease in the slip rate. Alternately, in folds formed with constant limb length and approxi-

mately constant slip and sedimentation rates, since uplift decreases with time, syntectonic sediments onlap in the first stages of evolution but then overlap the structure. Similar onlap-overlap relationships are found in the case of growth detachment folds formed with variable limb length when the slip rate decreases with time. Since the slip rate decreases with time the uplift rate also decreases. Therefore, the uppermost growth strata display subhorizontal dispositions and hardly show thickness variations across the fold. This makes it difficult to locate the boundary between growth and post-growth strata.

(4) The Pico del Aguila anticline began to develop in submarine conditions, starting at approximately 42.67 ± 0.02 Ma (Upper Lutetian). At 38.28 ± 0.02 Ma (Priabonian) the hinge became emergent but deformation continued until 36.68 ± 0.02 Ma (Bartonian) and possibly until 34.8 ± 1.72 Ma (Rupelian or Priabonian) always in subaerial environments. Therefore, the shortening lasted for about 7.87 ± 1.74 Ma. The total E–W shortening needed to form the Pico del Aguila anticline is about 2678 m, assuming that the growth-fold shortening was accommodated by limb rotation. If we assume a constant limb length detachment fold, the shortening rate was approximately constant at 0.35 ± 0.1 mm a^{-1}. If we assume a variable limb length detachment fold, the shortening rate decreased with time being as fast as 0.99 ± 0.01 mm a^{-1} during the initial stages of growth. The younger growth strata show little thickness variations across the fold and only slight evidence of deformation, indicating that the anticline uplift rate decreased through time (from 0.31 ± 0.08 mm a^{-1} during the first stages to zero). This makes it difficult to locate precisely the boundary between the syn- and post-growth sediments.

Acknowledgements—This study was supported by a post-doctoral fellowship (*Dynamics and kinematics of fault-related folding in thrust terranes*) within the Human Capital and Mobility programme funded by the Commission of the European Communities to which J. Poblet is indebted. It is also part of the *Fault Dynamics Project* sponsored by: ARCO British Ltd, BP Exploration, BRASOIL U.K., CONOCO U.K. Ltd, MOBIL North Sea Ltd and SUN Oil Britain. We also would like to acknowledge financial support from the Spanish Ministry for Education and Science and the British Council (Acción Integrada Hispano-Británica 1993/94 No. 45B: *Modelling of syn-sedimentary structures*). Bedding data were plotted using Richard Allmendinger's program to whom we are grateful. We thank Hector Millán for providing us with copies of his papers and Josep Serra-Kiel for helping us with the biostratigraphic data. We also thank Gautam Mitra, Shankar Mitra, Steven Wojtal, James Holl, Harvey Cohen, Myra Keep, Joao Keller, Ken McClay, Gary Nichols and Liz Thompson for constructive reviews of the manuscript.

REFERENCES

Almela, A. & Rios, J. M. 1951. Estudio geológico de la zona subpirenaica aragonesa y de sus sierras marginales. I Congreso Internacional del Pirineo de Estudios Pirenaicos, Zaragoza, 1951. *Geología* **3**, 327–350.

Anastasio, D. 1987. Thrusting, halotectonics and sedimentation in the External Sierras, Southern Pyrenees, Spain. Unpublished Ph.D. Thesis, Johns Hopkins University, Baltimore, MD.

Anastasio, D. 1992. Structural evolution of the External Sierra, Southern Pyrenees, Spain. In: *Structural Geology of Fold and Thrust Belts* (edited by Mitra, S. & Fisher, G. W.). The Johns Hopkins University Press, Baltimore, MD, pp. 239–251.

Angevine, C. L., Heller, P. L. & Paola, C. 1990. Quantitative sedimentary basin modeling. *Am. Ass. Petrol. Geol. Course Note Series* **32**.

Barnolas, A., Samsó, J. M., Teixell, A., Tosquella, J. & Zamorano, M. 1991. Evolución sedimentaria entre la cuenca de Graus-Tremp y la cuenca de Jaca-Pamplona. I Congreso del Grupo Español del Terciario, Vic, 1991. *Libro-Guía Excursión* **1**.

Barnolas, A., Teixell, A., Samsó, J. M. & Zamorano, M. 1992. Estructura y evolución sedimentaria del sector central de la cuenca surpirenaica. III Congreso Geológico de España, Salamanca, 1992. *Excursiones* **I**, 74–114.

Bentham, P. A. 1992. The tectono-stratigraphic development of the western oblique ramp of the South-Central Pyrenean thrust system, Northern Spain. Unpublished Ph.D. thesis, University of Southern California.

Bloch, R. B., Von Huene, R., Hart, P. E. & Wentworth, C. . 1993. Style and magnitude of tectonic shortening normal to the San Andreas fault across Pyramid Hills and Kettleman Hills South Dome, California. *Bull. geol. Soc. Am.* **105**, 464–478.

Burbank, D. W., Vergés, J., Muñoz, J. A. & Bentham, P. 1992. Coeval hindward- and forward-imbricating thrusting in the South Central Pyrenees, Spain: timing and rates of shortening and deposition. *Bull. geol. Soc. Am.* **104**, 3–17.

Burbank, D. W., Hogan P. J. & Bentham, A. P. In press. Chronology of foreland-basin evolution in the central and western Pyrenean foreland. In: *Tertiary Basins of Spain* (edited by Friend, P. & Dabrio, C.). Cambridge University Press, Cambridge, U.K.

Cámara, P. & Klimowitz, J. 1985. Interpretación geodinámica de la vertiente centro-occidental surpirenaica (cuenca de Jaca-Tremp). *Est. Geol.* **41**, 391–404.

Canudo, J.-I., Molina, E., Riveline, J., Serra-Kiel, J. & Sucunza, M. 1988. Les evenements biostratigraphiques de la zone prepyrenéenne d'Aragón (Espagne), de l'Eocène moyen a l'Oligocène inférieur. *Rev. Micropaléo.* **31**, 15–29.

Canudo, J.-I., Malagón, J., Melendez, A., Millán, H., Molina, E. & Navarro, J. J. 1991. Las secuencias deposicionales del Eoceno medio y superior de las Sierras exteriores (Prepirineo meridional aragonés). *Geogaceta* **9**, 81–84.

Chamberlin, R. T. 1910. The Appalachian folds of central Pennsylvania. *J. Geol.* **18**, 228–251.

Dahlstrom, C. D. A. 1990. Geometric constraints derived from the law of conservation of volume and applied to evolutionary models for detachment folding. *Bull. Am. Ass. Petrol. Geol.* **74**, 336–344.

DeCelles, P. G., Gray, M. B., Ridgway, K. D., Cole, R. B., Srivastava, P., Pequera, N. & Pivnik, D. A. 1991. Kinematic history of a foreland uplift from Paleocene synorogenic conglomerate, Beartooth Range, Wyoming and Montana. *Bull. geol. Soc. Am.* **103**, 1458–1475.

Déramond, J., Fischer, M., Hossack, J., Labaume, P., Séguret, M., Soula, J.-C., Viallard, P. & Williams, G. D. 1984. Field guide of conference trip to the Pyrenees. *Chevauchement et Déformation Conference, Tolouse*, 1984, pp. 1–28.

De Sitter, L. V. 1956. *Structural Geology*. McGraw-Hill, New York.

Dinarés, J. 1992. Paleomagnetisme a les unitats sudpirinenques superiors. Implicacions estructurals. Unpublished Ph.D. thesis, Universitat de Barcelona.

Dinarés, J., McClelland, E. & Santanach, P. 1992. Contrasting rotations within thrust sheets and kinematics of thrust tectonics as derived from palaeomagnetic data: an example from the Southern Pyrenees. In: *Thrust Tectonics* (edited by McClay, K.). Champman & Hall, London, pp. 265–275.

Dobson, J. 1990. The dynamics of foreland fold and thrust belts, Southern Canadian Rocky Mountains, SW Alberta, Canada. Unpublished Ph.D. thesis, University of London.

Epard, J.-L. & Groshong, R. H. 1993. Excess area and depth of detachment. *Bull. Am. Ass. Petrol. Geol.* **77**, 1291–1302.

Fischer, M. P., Woodward, N. B. & Mitchell, M. M. 1992. The kinematics of break-thrust folds. *J. Struct. Geol.* **14**, 451–460.

Garrido, A. 1973. Estudio geológico y relación entre tectónica y sedimentación del secundario y terciario de la vertiente meridional pirenaica en su zona central. Unpublished Ph.D. thesis, Universidad de Granada.

Hardy, S. & Poblet, J. 1994. Geometric and numerical model of progressive limb rotation in detachment folds. *Geology* **22**, 371–374.

Hardy, S. & Poblet, J. 1995. The velocity description of deformation. Paper 2: sediment geometries associated with fault-bend and fault-propagation folds. *Marine Petrol. Geol.* **12**, 165–176.

Hardy, S., Poblet, J., McClay, K. & Waltham, D. 1995. Mathematical modelling of growth strata associated with fault-related fold structures. *Spec. Publ. Geol. Soc.* (in press).

Harland, W. B., Armstrong, R. L., Cod, A. G., Craig, L., Smith, A. & Smith, D. G. 1990. *A Geologic Time Scale* 1989. Cambridge University Press, Cambridge, U.K.

Hogan, P. J. 1991. Geochronologic, tectonic, and stratigraphic evolution of the Southwest Pyrenean Foreland Basin, Northern Spain. Unpublished Ph.D. thesis, University of Southern California.

Hogan, P. J., Burbank, D. W. & Puigdefábregas, C. 1988. Magnetostratigraphic chronology of the sedimentologic and tectonic evolution of the Jaca basin, Southwestern Pyrenees. *Symposium on the Geology of the Pyrenees and Betics, Barcelona, 1988.* Abstracts **76**.

Jackson, M. P. A. & Talbot, C. J. 1994. Advances in salt-tectonics. In: *Continental Deformation* (edited by Hancock, P. L.). Pergamon Press, Oxford, pp. 159–179.

Jamison, W. R. 1987. Geometric analysis of fold development in overthrust terranes. *J. Struct. Geol.* **9**, 207–219.

Martínez, B., Casas, A. M. & Millán, H. 1995. Paleostresses associated with thrust sheet emplacement and related folding in the Southern Central Pyrenees, Huesca, Spain. *J. Geol. Soc.* **152**, 353–364.

McElroy, R. 1990. Thrust kinematics and syntectonic sedimentation: the Pyrenean frontal ramp, Huesca, Spain. Unpublished Ph.D. thesis, University of Cambridge.

Medwedeff, D. A. 1989. Growth fault-bend folding at Southeast Lost Hills, San Joaquin Valley, California. *Bull. Am. Ass. Petrol. Geol.* **73**, 54–67.

Medwedeff, D. A. 1992. Geometry and kinematics of an active, laterally propagating wedge thrust, Wheeler Ridge, California. In: *Structural Geology of Fold and Thrust Belts* (edited by Mitra, S. & Fisher, G. W.). The Johns Hopkins University Press, Baltimore, MD, pp. 3–28.

Millán, H., Parés, J. M. & Pocoví, A. 1992. Modelización sencilla de la estructura del sector occidental de las sierras marginales aragonesas (Prepirineo, provincias de Huesca y Zaragoza). III Congreso Geológico de España, Salamanca, 1992. *Simposios* **2**, 140–149.

Millán, H., Aurell, M. & Melendez, A. 1994. Synchronous detachment folds and coeval sedimentation in the Prepyrenean External Sierras (Spain): a case study for a tectonic origin of sequences and system tracts. *Sedimentology* **41**, 1001–1024.

Millán, H., Pocoví, A. & Casas, A. M. 1995. El frente de cabalgamiento surpirenaico en el extremo occidental de las Sierras Exteriores. *Rev. Soc. Geol. España* (in press).

Mitra, S. & Namson, J. S. 1989. Equal-area balancing. *Am. J. Sci.* **289**, 563–599.

Mount, V. S., Suppe, J. & Hook, S. 1990. A forward modeling strategy for balancing cross sections. *Bull. Am. Ass. Petrol. Geol.* **74**, 521–531.

Muñoz, J. A. 1992. Evolution of a continental collision belt: ECORS–Pyrenees crustal balanced cross-section. In: *Thrust Tectonics* (edited by McClay, K.). Chapman & Hall, London, pp. 235–246.

Muñoz, J. A., McClay, K. & Poblet, J. 1994. Synchronous extension and contraction in frontal thrust sheet of the Spanish Pyrenees. *Geology* **22**, 921–924.

Pueyo-Morer, E. L., Parés, J. M., Millán, H. & Pocoví, A. 1994. Evidencia magnetotectónica de la rotación de las Sierras Exteriores Altoaragonesas. II Congreso del Grupo Español del Terciario, Jaca, 1994. *Comunicaciones*, 185–189.

Puigdefábregas, C. 1975. La sedimentación molásica en la cuenca de Jaca. *Pirineos* **104**, 1–88.

Riba, O. 1976. Syntectonic unconformities in the Alto Cardener, Spanish Pyrenees: a genetic interpretation. *Sediment. Geol.* **15**, 213–233.

Sclater, J. G. & Christie, P. A. F. 1980. Continental stretching: an explanation of the post-Mid-Cretaceous subsidence of the central North Sea basin. *J. geophys. Res.* **85**, 3711–3739.

Séguret, M. 1972. *Etude Tectonique des Nappes et Séries décollées de la Partie Centrale du Versant Sud des Pyrenées*. Publications Ustela, Montpellier.

Shaw, J. H. & Suppe, J. 1994. Active faulting and growth folding in the eastern Santa Barbara Channel, California. *Bull geol. Soc. Am.* **106**, 607–626.

Soler, M. & Puigdefábregas, C. 1970. Líneas generales de la geología del Alto Aragón occidental. *Pirineos* **96**, 5–20.

Suppe, J. 1983. Geometry and kinematics of fault-bend folding. *Am. J. Sci.* **282**, 684–721.

Suppe, J. & Medwedeff, D. A. 1990. Geometry and kinematics of fault-propagation folding. *Eclog. geol. Helv.* **83**, 409–454.

Suppe, J., Chou, S. T. and Hook, S. C. 1992. Rates of folding and faulting determined from growth strata. In: *Thrust Tectonics* (edited by McClay, K.). Chapman & Hall, London, pp. 105–121.

Vendeville, B. C. & Jackson, M. P. A. 1992. The rise of diapirs during thin-skinned extension. *Marine Petrol. Geol.* **9**, 331–353.

Wilson, G. 1967. The geometry of cylindrical and conical folds. *Proc. geol. Ass.* **78**, 179–210.

APPENDIX

Derivation of equation (1) *to calculate the depth to detachment*

From angular relationships, we know that the area of the core of a symmetrical chevron detachment fold is (Fig. 2):

$$\frac{(L \cos \vartheta + L \cos \vartheta)H}{2}. \tag{A1}$$

Inspection of Fig. 2 shows that

$$H = L \sin \vartheta. \tag{A2}$$

Substituting equation (A2) into equation (A1) and rearranging, the fold core area becomes

$$L^2 \cos \vartheta \sin \vartheta. \tag{A3}$$

Equating this expression to the slip times the depth to detachment, we obtain equation (1).